# An Underactuated Active Transfemoral Prosthesis With Series Elastic Actuators Enables Multiple Locomotion Tasks

Ilaria Fagioli, Francesco Lanotte, *Member, IEEE*, Tommaso Fiumalbi, Andrea Baldoni, Alessandro Mazzarini, Filippo Dell'Agnello, Huseyin Eken, *Graduate Student Member, IEEE*, Vito Papapicco, Tommaso Ciapetti, Alessandro Maselli, Claudio Macchi, Sofia Dalmiani, Angelo Davalli, Emanuele Gruppioni, *Member, IEEE*, Emilio Trigili, *Member, IEEE*, Simona Crea, *Member, IEEE*, and Nicola Vitiello, *Member, IEEE*

***Abstract*—Robotic lower limb prostheses have the power to revolutionize mobility by enhancing gait efficiency and facilitating movement. While several design approaches have been explored to create lightweight and energy-efficient devices, the potential of underactuation remains largely untapped in lower limb prosthetics. Taking inspiration from the natural harmony of walking, in this article, we have developed an innovative active transfemoral prosthesis. By incorporating underactuation, our design uses a single power actuator placed near the knee joint and connected to a differential mechanism to drive both the knee and ankle joints. We conduct comprehensive benchtop tests and evaluate the prosthesis with three individuals who have above-knee amputations, assessing its performance in walking, stair climbing, and transitions between sitting and standing. Our evaluation focuses on gathering position and torque data recorded from sensors integrated into the prosthesis and comparing these measurements to biomechanical data of able-bodied locomotion. Our findings highlight the promise of underactuation in advancing lower limb prosthetics and demonstrate the feasibility of our knee–ankle underactuated design in various tasks, showcasing its ability to replicate natural movement.**

***Index Terms*—Powered prostheses, series elastic actuator (SEA), underactuation, wearable robotics.**

Manuscript received 17 January 2024; revised 29 April 2024; accepted 25 May 2024. Date of publication 17 June 2024; date of current version 1 July 2024. This paper was recommended for publication by Associate Editor Michael Posa and Editor Sven Behnke upon evaluation of the reviewers' comments. This work was supported by the Istituto Nazionale per l'Assicurazione Contro gli Infortuni sul Lavoro (INAIL), within the MOTU and MOTU++ Projects under Grant n° PPR-AI 1-2 and Grant PR19-PAI-P2. *(Ilaria Fagioli, Francesco Lanotte, and Tommaso Fiumalbi contributed equally to this work.) (Corresponding author: Ilaria Fagioli.)*

This work involved human subjects or animals in its research. Approval of all ethical and experimental procedures and protocols was granted by Ethics Committees of Area Vasta Toscana Centro under Application No. 16677, and Area Vasta Emilia Centro under Application No. 19168, and performed in line with the Declaration of Helsinki.

Ilaria Fagioli, Andrea Baldoni, Alessandro Mazzarini, Filippo Dell'Agnello, Huseyin Eken, Sofia Dalmiani, and Emilio Trigili are with The BioRobotics Institute, Scuola Superiore Sant'Anna, 56025 Pontedera, Italy, and also with the Department of Excellence in Robotics and AI, Scuola Superiore Sant'Anna, 56127 Pisa, Italy (e-mail: ilaria.fagioli@santannapisa.it).

Francesco Lanotte was with The BioRobotics Institute, 56025 Pontedera, Pisa, Italy. He is now with the Technology and Innovation Hub (tiHUB), Shirley Ryan AbilityLab, Chicago, IL 60611 USA, and also with the Max Nader Laboratory for Rehabilitation Technologies and Outcomes Research, Shirley Ryan AbilityLab, Chicago, IL 60611 USA.

Tommaso Fiumalbi and Vito Papapicco were with The BioRobotics Institute, Scuola Superiore Sant'Anna, 56025 Pontedera, Pisa, Italy.

Tommaso Ciapetti and Claudio Macchi are with the Institute of Recovery and Care of Scientific Character (IRCCS), Fondazione Don Carlo Gnocchi, 50143 Firenze, Italy.

Alessandro Maselli was with the Institute of Recovery and Care of Scientific Character (IRCCS), Fondazione Don Carlo Gnocchi, 50143 Firenze, Italy.

Angelo Davalli and Emanuele Gruppioni are with Centro Protesi Inail, Vigorso di Budrio, 40054 Bologna, Italy.

Simona Crea and Nicola Vitiello are with The BioRobotics Institute, Scuola Superiore Sant'Anna, Pontedera, Italy, also with the Department of Excellence in Robotics and AI, Scuola Superiore Sant'Anna, 56127 Pisa, Italy, also with the Institute of Recovery and Care of Scientific Character (IRCCS), Fondazione Don Carlo Gnocchi, 50143 Firenze, Italy, and also with IUVO S.r.l., 56025 Pontedera, Pisa, Italy.

This article has supplementary downloadable material available at https://doi.org/10.1109/TRO.2024.3415228, provided by the authors.

Digital Object Identifier 10.1109/TRO.2024.3415228

## Nomenclature

| | |
|---|---|
| BER | Brakes engagement regulator. |
| FC | Foot contact. |
| FF | Foot flat. |
| FO | Foot off. |
| FPGA | Field programmable gate array. |
| FSM | Finite-state machine. |
| HO | Heel off. |
| MF | Maximum thigh flexion. |
| MS | Mid swing. |
| SEA | Series elastic actuator. |
| SOM | System on module. |
| SPF | Sensorized prosthetic foot. |
| vGRF | Vertical ground reaction force. |
| yCOP | Center of pressure along the antero–posterior axis. |

## I. Introduction

IMPROVEMENTS in the quality of treatment are leading to a reduced incidence of lower limb amputation [1], [2]. Nonetheless, it is expected that more than 3 million people will undergo amputation by 2050 in the USA alone [3]. Among lower limb amputations, above-knee (i.e., transfemoral) amputation can be highly debilitating, as transfemoral amputees typically experience slower walking speeds [4], an elevated risk of balance loss [5], and up to 2.5 times higher energetic costs of walking

than nonamputees [6]. These factors can significantly limit mobility and impair a person's quality of life [7]. The prevalence of this issue is particularly worrisome among dysvascular patients [8], who constitute the largest proportion of individuals with transfemoral amputations [9], [10].

Most commercially available transfemoral prostheses are passive or semiactive devices, which do not power the whole gait cycle [11]. This determines alterations in the biomechanics of locomotion [12] that can cause secondary complications, such as chronic back pain and osteoporosis [13], [14].

Active (or robotic) prostheses are equipped with actuators that allow the replication of the main biomechanical functions of the missing limb. As a result, these devices have the potential to improve prosthetic gait efficiency and facilitate the execution of demanding tasks, such as climbing stairs and transitioning between sitting and standing [15], [16], [17]. Different design approaches have been explored to efficiently match the torque and speed performance of human joints. Elastic elements in series and in parallel to motors have been used to simulate the biological joint impedance and reduce the torque requirements of the actuation unit [18], [19], [20], [21], [22]. High-torque actuators have been coupled with low reduction ratio gears to decrease output impedance and increase back drivability [20], [23]. Hybrid design strategies [24], [25] and variable transmission mechanisms [26], [27] have been proposed to limit the weight of prosthetic devices.

Interestingly, hand prostheses [28], [29], [30] and powered exoskeletons [31], [32], [33], [34] have extensively investigated the use of underactuation, resulting in multijoint and lightweight devices. In particular, differential mechanisms have been used to mechanically couple the actuation of multiple joints that are coordinated during the execution of a task, such as the digits during grasping [28], [30], the hip joints during walking [35], or the trunk and hips during lifting tasks [32], [33]. Recently, an underactuated mechanism was introduced in the design of an ankle/toe prosthesis to match the synergy of the metatarsal joint and promote energy recovery [36], [37]. In this framework, a concept for an underactuated transfemoral prosthesis could leverage the knee–ankle kinematic coordination in the main locomotion tasks [38]. The possibility to distribute power between the two joints complies with the variable power requirements they exhibit across different activities and gait phases [39].

This article presents the MOTU Transfemoral Synergy Prosthesis (SynPro), a knee–ankle prosthesis driven by a single power actuator. To the best of our knowledge, this prototype represents the first instance of a prosthesis incorporating a differential mechanism to convey the power of a single motor to both the knee and ankle joints. During a substantial portion of the gait cycle, in which the knee flexion/extension is coupled to the ankle plantarflexion/dorsiflexion, the differential mechanism enables the simultaneous movement of both joints through the single power actuator. Additionally, the prosthesis incorporates a braking system, driven by two low-power servoactuators, to manage the coupling between the two joints and to independently power a single joint. This feature extends the prosthesis' functionality beyond walking, enabling users to perform tasks such as stair negotiation and sit/stand transitions. Furthermore, each joint incorporates series elasticity, resulting in a force-sensing architecture for compliant interaction with the ground [40]. Benchtop tests and experiments conducted with three individuals with above-knee amputation demonstrated that the presented underactuated prosthesis can assist in performing essential locomotion tasks, such as level-ground walking, stair ascending and descending, and sit/stand transitions.

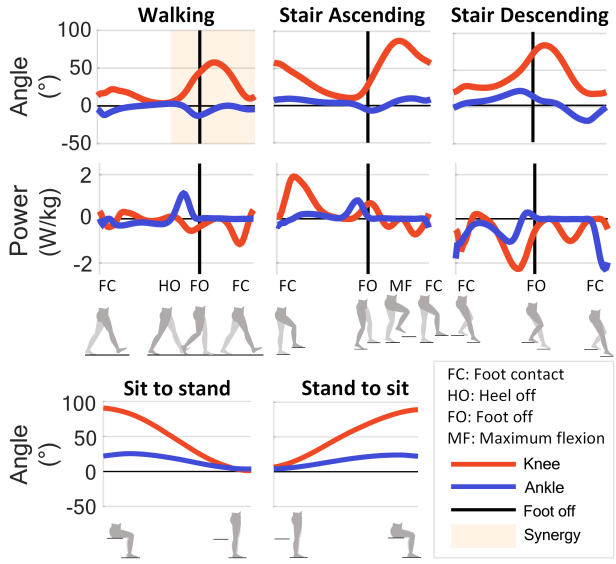


Fig. 1. Kinematics and power profiles of the knee and ankle joints during level-ground walking, stair ascending, stair descending, and kinematic profiles of the joints during sit-to-stand and stand-to-sit. Data adapted from [39] and [56].

The rest of this article is organized as follows. Section II describes the kinematic synergies and power requirements that inspired the SynPro design, as well as the mechatronic architecture and control system of the prosthesis. Sections III and IV report the benchtop tests and experiments with subjects with transfemoral amputations, respectively. The results are discussed in Section V. Finally, Section VI concludes this article.

## II. SynPro Design

### A. Kinematic Synergies and Power Requirements of the Knee and Ankle Joints

Human gait is a complex activity that requires the coordination of multiple body segments [41]. In walking, the coordinated movement pattern—that we refer to as kinematic synergies—between the knee and the ankle joints is particularly evident from the heel off (HO) event (see the yellow patch in Fig. 1) [42]. During the late stance, from HO to foot off (FO), the knee flexion is coordinated with the ankle plantarflexion to control the lifting of the leg. During this phase, the ankle generates a peak of power, while the knee dissipates power. In the swing phase, after reaching the peak flexion angle, the knee extends in coordination with the ankle dorsiflexion to ensure foot clearance. The knee acts again as a damper, showcasing a peak of energy absorption in late swing.

Stair negotiation tasks and sit/stand transitions exhibit different patterns of movement of the knee and ankle joints, as the knee typically takes the lead in terms of movement and power exertion to support the body's weight [43]. At the FC of

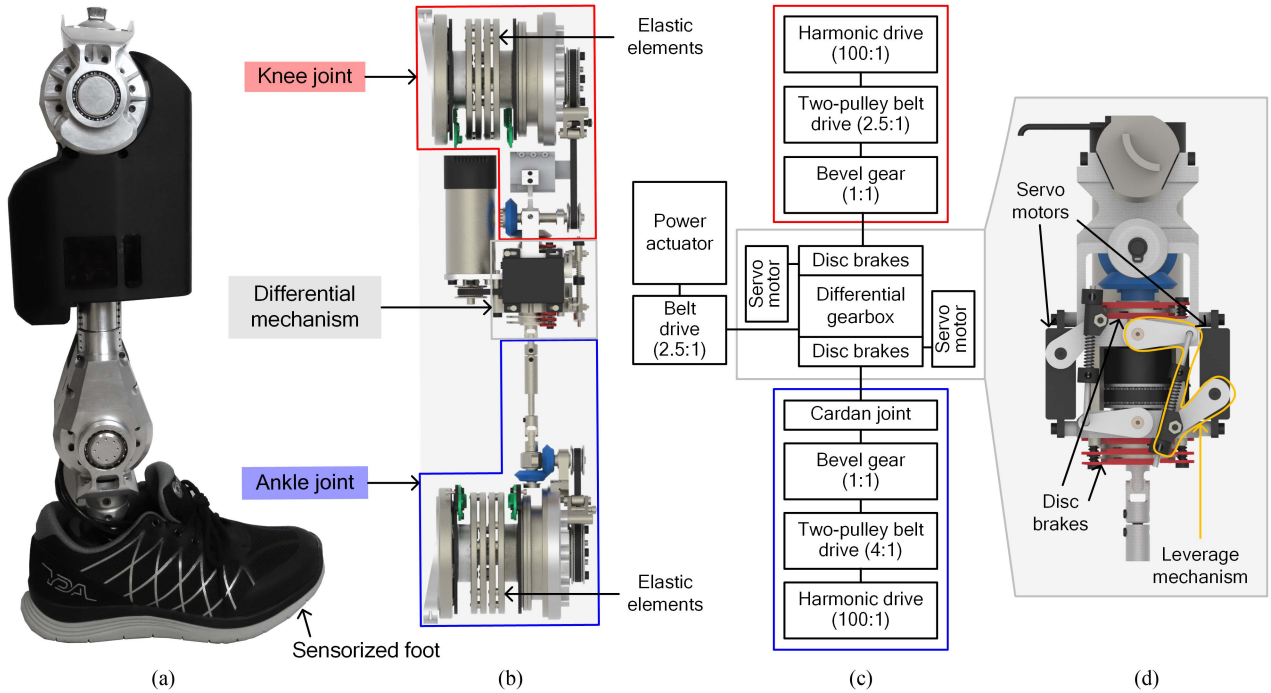


Fig. 2. (a) Overview of the SynPro. (b) Frontal CAD view of the SynPro's mechanical components. (c) Schematic representation of the transmission stages. (d) Lateral CAD view of the differential mechanism.

stair ascending, the knee joint is flexed and the ankle is slightly dorsiflexed. During stair ascent, the ankle plantarflexes, while the knee extends, generating significant power to lift the user's body upward. In contrast, stair descent is characterized by energy absorption and dissipation. The knee joint flexes throughout descent and achieves maximum flexion right after FO. The ankle joint remains dorsiflexed for most of the stance phase and starts to plantarflex in late stance. During sit/stand transitions, the knee extends and flexes to lift and lower the body, and the ankle joint plantarflexes and dorsiflexes to provide stability and balance.

The analysis of biomechanical profiles reveals that the combined knee and ankle power is lower than the total power required to separately actuate the two joints. This suggests the feasibility of employing a single actuator to power both joints, thereby reducing the mechanical and electrical components associated with a second power actuator. Furthermore, leveraging a single power actuator could foster the synergistic movement between the knee and ankle joints, promoting more efficient and coordinated locomotion.

### B. Overview of the SynPro

The system, as shown in Fig. 2(a) and (b), includes the knee and ankle joints, the power unit, the battery, the electronic board, and a sensorized foot, a part of the multimodal sensory system of the prosthesis. The electromagnetic power unit is coupled with a differential gearbox equipped with disc brakes. The differential mechanism and the transmission chain of the SynPro enable the simultaneous actuation of knee flexion with ankle plantarflexion and knee extension with ankle dorsiflexion. This design choice aims to harness the synergic movement of the knee and ankle joints during walking, which is the most common locomotion mode [39]. The disc brakes located at the outputs of the differential gearbox [see Fig. 2(c) and (d)] serve two essential functions. First, during the synergistic actuation of the knee and ankle joints, they ensure that the joints remain within the physiological range of movement. Second, when the synergic motion is not required, such as during stair negotiation, fully engaging a disc brake blocks the movement of a joint, thereby enabling the motor power to actuate only the opposite joint. When a joint is braked, the series elasticity fosters compliance, energy absorption, and shock tolerance, contributing to the overall stability and safety of the SynPro [43], [44]. The entire system weighs 6.2 kg, including the battery pack and the wiring. The requirements and characteristics of the prosthesis are summarized in Table I.

TABLE I
REQUIREMENTS AND CHARACTERISTICS OF THE SYNPRO

| | | |
|---|---|---|
| User | Max Weight | 100 kg |
| Knee joint | Max Torque | 110 Nm |
| | Speed | ~200 °/s |
| | RoM | -5° – +120° |
| Ankle joint | Max Torque | 120 Nm |
| | Speed | ~200 °/s |
| | RoM | -35° – +35° |
| Weight of the device | | 6.2 kg |
| Length of the device (distance between the joints) | | 295 – 341 mm |
| Maximum power | | 200 W |
| Power supply | | Battery pack |

### C. Power Unit and Differential Gearbox

The SynPro is powered by a 200 W brushless dc motor (EC 4-pole 30, Maxon Motor, Sachseln, Switzerland), equipped with an incremental encoder (1024 ppr, ENC 16 EASY, Maxon Motor, Sachseln, Switzerland). The motor is placed along the longitudinal axis of the prosthesis, close to the knee joint to limit the device's distal mass. A belt drive (reduction ratio 2.5:1) transfers the mechanical power from the motor axis to the input axis of the differential gearbox, which is based on a patent-pending concept [45]. The power from the input axis is distributed between the two output axes (connected to the knee and ankle joints) by the differential gearbox, whose working principle is described by Willis' equation

$$\Omega = \frac{\omega_k + \omega_a}{2} \tag{1}$$

where $\Omega$ is the angular speed of the input shaft (i.e., planet gear carrier), and $\omega_a$ and $\omega_k$ are the angular speeds of the two output shafts, which depend on the engagement status of the disc brakes. Assuming negligible friction and inertial terms, when the disc brakes are disengaged, the input torque $\tau$ from the motor is equally split to the output shafts of the gearbox [33]. In a preliminary bench testing phase, we verified the relation between the motor velocity and the velocity at the outputs of the differential gearbox when both joints were free to move and when one brake was engaged. We determined that possible backslash in the transmission did not compromise the validity of Willis' law. Moreover, when commanding a current to the motor, we compared the torque at the input and outputs of the differential mechanism in static conditions (i.e., with the prosthesis' outputs blocked and the disk brakes disengaged) and empirically quantified the transmission friction torque to be approximately 10%–20% of the motor torque. When engaged, a disc brake will exert a braking torque $\tau_f$ on the respective output of the differential gearbox. If the brake of the knee is engaged, the motor torque is transmitted at the two outputs of the differential gearbox as follows:

$$\begin{cases} \tau_k = \frac{\tau}{2} - \tau_{f_{\text{knee}}} \cdot \frac{|\omega_k - \omega_a|}{\omega_k - \omega_a} \\ \tau_a = \frac{\tau}{2} + \tau_{f_{\text{knee}}} \cdot \frac{|\omega_k - \omega_a|}{\omega_k - \omega_a} \end{cases} \tag{2}$$

where $\tau_k$ and $\tau_a$ are the torques at the outputs of the differential gearbox at the knee and ankle sides (i.e., before the transmission stages). The analogous relation holds if the ankle brake is engaged. When the braking torque equals the torque contribution of the motor $\frac{\tau}{2}$, the angular speed of the braked output shaft is zero, and no motor torque is transmitted to the braked prosthetic joint. The disc brakes are controlled by two servomotors (D145SW, Hitec, San Diego, CA, USA) through leverage mechanisms, one of which is highlighted in Fig. 2(d). The output of each servomotor can be moved in the range 0°–120°. For each brake, two positions were empirically determined: $B_e$ when the brake is engaged (i.e., the respective joint cannot be moved), and $B_d$ when the brake is disengaged (i.e., the joint can be actuated or moved by an external force).

### D. Knee and Ankle Joints

The transmission chain going from the output of the differential gearbox to the knee joint is schematically shown in the red box in Fig. 2(c). The rotary motion of the output shaft of the differential gearbox is transferred from the longitudinal to the transversal axis of the prosthesis by a bevel gear mechanism (reduction ratio 1:1). The output of the bevel gear is the input to a two-pulley belt-drive mechanism (reduction ratio 2.5:1), whose distal pulley is connected to a harmonic drive (CSD-25-100-2A-GR, reduction ratio 100:1, Harmonic Drive, Limburg, Germany), coaxial with the axis of the knee joint. Four custom torsional springs are connected in series to the output of the harmonic drive. The knee joint can move between $-5°$ and 120° (flexion positive).

The transmission chain going from the output of the differential gearbox to the ankle joint is schematically shown in the blue box in Fig. 2(c). The output shaft of the differential gearbox is linked to a Cardan joint with an adjustable length (stroke of 52 mm). The motion is transferred from the longitudinal to the transversal axis of the prosthesis through a bevel gear (reduction ratio 1:1), coupled with a two-pulley belt drive (reduction ratio 4:1) and a harmonic drive (CSD-25-100-2A-GR, reduction ratio 100:1, Harmonic Drive, Limburg, Germany). The ankle joint can move between $-35°$ and 35° (dorsiflexion positive).

The elastic elements at the knee and ankle joints were designed to have an equivalent stiffness of 580 N·m/rad [46], comparable with the quasi-stiffness of a healthy joint (ranging between 200 and 700 N·m/rad in walking tasks [47], [48]). The springs serve as sensing elements that measure the torque after the transmission stages of the joints, inherently accounting for the transmission losses.

### E. Multimodal Sensory System

The sensory apparatus of the SynPro includes the following:

1) two absolute encoders per joint (20-bit resolution, Aksim2, RLS, Komenda, Slovenia) to measure the deflection of the elastic element and the output joint position, needed to compute the torque applied to the joint with a resolution of 3.4 mN·m;
2) a remote nine-axis inertial measurement unit (IMU) (MPU9250, TDK/InvenSense, San Jose, CA, USA) to monitor the movement of the residual limb;
3) an onboard IMU (iNemo, LSM9DS1, STMicroelectronics, Geneva, Switzerland);
4) a sensorized prosthetic foot (SPF).

The SPF consists of a commercial prosthetic foot (LP VariFlex, Össur, Reykjavik, Iceland), which embeds a 9-axis IMU (MPU9250, TDK/InveSense, San Jose, CA, USA) and 16 pressure-sensitive elements based on optoelectronic technology [49], [50], [51], [52]. The sensing elements are organized in a series of scalable printed circuit board (PCB) matrices along the foot's antero–posterior axis. Sensors are placed in the most loaded plantar regions (i.e., the heel and the forefoot) to enhance the detection of gait events, such as foot contact (FC) and FO. The signals from the pressure-sensitive elements of the SPF and the IMU are acquired using a data acquisition board enclosed in

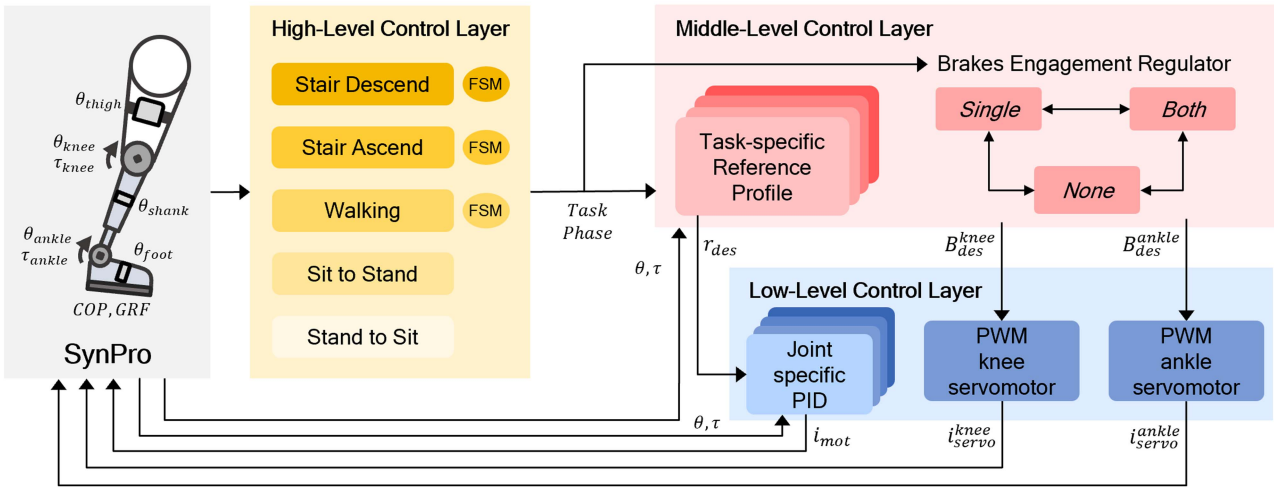


Fig. 3. Hierarchical control architecture of the SynPro. Using signals from the onboard sensors, the high-level control layer decodes locomotion-related phases through FSMs. Depending on the detected phase, the middle-level control layer computes a reference profile and manages the engagement of the brakes through the BER. Based on the reference profile and the desired brake configuration, the low-level control layer computes the current to the motor through PID regulators and the current to the servomotors that control the disc brakes.

a plastic box, which communicates with the electronic board of the SynPro through differential serial peripheral interface buses.

### F. Electronics

The electronic board of the SynPro is composed of two layers: a main board and an actuator power board. The main board embeds the control logic unit, i.e., a system on module (SOM) SbRIO-9651 (National Instruments, Austin, TX, USA) equipped with a Xilinx Zynq-7020 containing a field programmable gate array (FPGA) and a dual-core ARM processor running an NI real-time operating system. The SOM connects via Wi-Fi to a remote laptop for online monitoring of the prosthesis' functioning. In addition, the main board collects the signals coming from the prosthesis sensors. The actuator power board includes the servoamplifier components for the main motor (Elmo Gold Twitter 30 A/60 V, Maxon Motor, Sachseln, Switzerland) and for the two servomotors, and the power supply management unit (dc/dc, Traco Power, Baar, Switzerland). The prosthesis is powered by a commercial battery pack (Li-Ion, eight cells, 28.8 V–2250 mAh, Inspired Energy, Kirkham, U.K.). An external emergency button can be operated to disable the motor driver in case of adverse events (safe torque off) [53].

### G. Control System

The control system of the SynPro employs a three-layered hierarchical architecture (see Fig. 3). In the high-level control layer, task-specific finite-state machines (FSMs) decode locomotion-related phases from data collected by the onboard sensors, the IMUs, and the SPF. Based on the task and decoded phase, the middle-level control layer computes the desired position or torque reference. This control layer includes a software module, the brake engagement regulator (BER), which manages the engagement of the brakes through the servomotors. Both the high-level and middle-level control layers run on the real-time processor at a frequency of 100 Hz.

The low-level control layer computes the current $i_{\text{mot}}$ required by the power actuator to track a desired reference $r_{\text{des}}$, and the currents ($i_{\text{servo}}^{\text{knee}}$ and $i_{\text{servo}}^{\text{ankle}}$) to set the servomotors in the desired positions ($B_{\text{des}}^{\text{knee}}$ and $B_{\text{des}}^{\text{ankle}}$, respectively). Four proportional–integral–derivative (PID) regulators, two for the knee joint and two for the ankle joint, track either joint position or joint torque depending on the monitored feedback variable. Based on the error between the desired reference and the measured feedback variable, the PID regulators return a current in the range of $[-20, 20]$ A to drive the power actuator. The low-level control layer runs on the FPGA at a frequency of 1 kHz.

*1) Brakes Engagement Regulator:* The BER is a software module designed to regulate the engagement of the knee and ankle brakes during the functioning of the SynPro. The BER includes three brakes' configurations: *Both*, *Single*, and *None*. In the *Both* configuration, both brakes are fully engaged and the current to the power actuator is set to zero. This configuration is useful for weight-bearing tasks since it implies almost null power dissipation. In the *Single* configuration, one joint is completely braked, while the other joint is controlled by a PID regulator. When the system switches the behavior of the two joints (the braked joint becomes the controlled one and vice-versa), the BER manages the noninstantaneous dynamics of the brakes by introducing a time window in which both brakes are engaged before disengaging the brake of the joint that will be controlled. The duration of the time window was experimentally set to 130 ms.

Finally, the *None* configuration is used when the knee and ankle joints are synergically actuated (i.e., one joint is controlled by a PID regulator, while the opposite joint moves due to the mechanical coupling with the controlled joint). In this configuration, the BER maintains the movement of the noncontrolled joint between a maximum flexion angle $\alpha_{\text{flex}}$ and a maximum

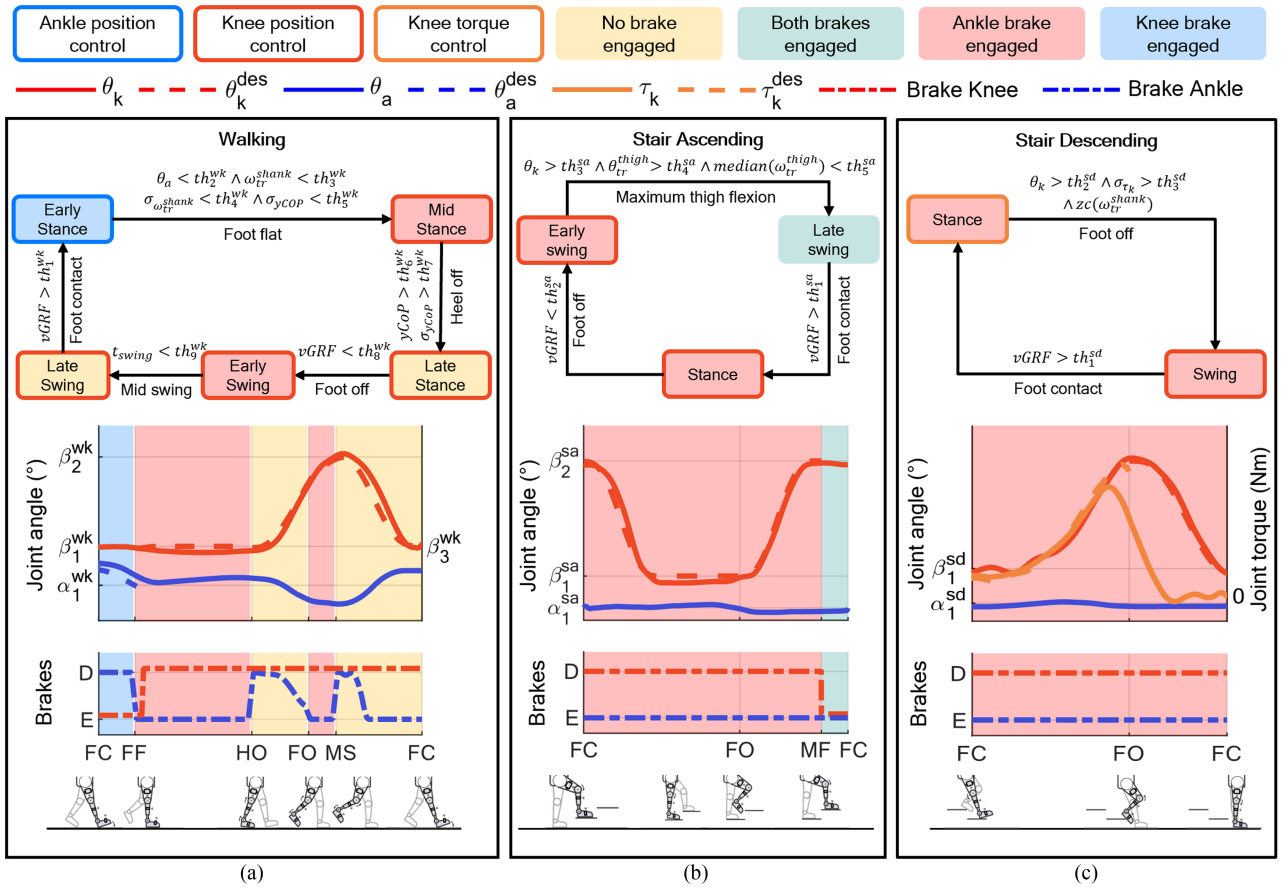


Fig. 4. FSMs for (a) walking, (b) stair ascending, and (c) stair descending. The upper row shows the FSMs' phases and the phase transition conditions. The lower row displays the joint variables and the brakes' engagement for each locomotion task and respective phases. These data depict a single stride recorded during preliminary tests with the prosthesis. D stands for disengaged, and E for engaged.

extension angle $\alpha_{\text{ext}}$. Given the position $\theta_{\text{start}}$ of the noncontrolled joint at the start of the *None* configuration, the desired position of its servo $B_{\text{des}}$ is computed as follows:

$$B_{\text{des}}\ (t) = \frac{B_e - B_d}{\alpha_{\text{dir}} - \theta_{\text{start}}} \cdot (\theta\,(t) - \theta_{\text{start}}) + B_d \qquad (3)$$

where $\alpha_{\text{dir}}$ is equal to $\alpha_{\text{flex}}$ if the joint is flexing or to $\alpha_{\text{ext}}$ if the joint is extending. The proportional engagement of the brake described in (3) was designed to progressively decelerate the noncontrolled joint when it approaches the boundary positions.

### H. FSMs and Reference Computation

Task-specific FSMs decode the locomotion-related phases of walking, stair ascending, and stair descending. At the current development stage, transitions between different locomotion tasks are manually triggered by the experimenter.

*1) Level-Ground Walking:* The walking FSM, as shown in Fig. 4(a), detects in real time the following events.

1) *FC*: The vertical ground reaction force vGRF estimated by the SPF is above a threshold $\text{th}_1^{wk}$ [49], [50].
2) *Foot flat (FF)*: The foot lies on the ground in a quasi-static position. This event is detected by verifying that the ankle joint angle $\theta_a$, the angular speed measured by the shank IMU $\omega_{tr}^{\text{shank}}$, and the standards' deviations of the same angular speed $\sigma_{\omega_{tr}^{\text{shank}}}$ and of the center of pressure $\sigma_{y\text{CoP}}$ over five samples are below set thresholds ($\text{th}_{2-5}^{wk}$).
3) *HO*: The anterior–posterior coordinate of the center of pressure $y$CoP estimated by the SPF [50] and its standard deviation over five samples $\sigma_{y\text{CoP}}$ are above the thresholds $\text{th}_6^{wk}$ and $\text{th}_7^{wk}$, respectively.
4) *FO*: The vGRF is below a threshold $\text{th}_8^{wk}$.
5) *Mid swing (MS)*: A set time $\text{th}_9^{wk}$ has elapsed from FO.

These events segment the gait cycle into five phases. During early stance (FC to FF), the ankle joint is plantarflexed to an angle $\alpha_1^{wk}$ to avoid foot slap. To increase the prosthesis' stability at FC, the knee joint is braked, promoting the absorption of the impact energy by the elastic element. During mid stance (FF to HO), the ankle joint is braked so that its elastic elements (i.e., the series springs and the prosthetic foot) can compress and store energy. In this phase, the knee brake is disengaged, and the joint is commanded at an angle $\beta_1^{wk}$. In late stance (HO to FO), the knee flexion is commanded toward an angle $\beta_2^{wk}$, while the ankle joint plantarflexes due to the coupling with the knee joint, and the BER prevents it from reaching nonphysiological positions. In early swing (FO to MS), the ankle joint is braked, while the knee flexes to ensure foot clearance. In late swing (MS

to FC), the BER is in the *None* configuration: the knee extends up to the angle $\beta_3^{wk}$, while the ankle dorsiflexes synergically [see Fig. 4(a)].

*2) Stair Ascending:* The stair ascending FSM decodes the following gait events, as shown in Fig. 4(b).

1) *FC*: The vGRF is greater than a threshold $\text{th}_1^{sa}$.
2) *FO*: The vGRF is lower than a threshold $\text{th}_2^{sa}$.
3) *Maximum thigh flexion (MF)*: The leg is lifted to position the foot on the next step. This event is detected when three conditions are verified. The knee joint angle $\theta_k$ and the rotation angle around the transversal axis estimated by the thigh IMU $\theta_{tr}^{\text{thigh}}$ surpass thresholds $\text{th}_3^{sa}$ and $\text{th}_4^{sa}$, respectively. Then, the thigh IMUs angular speed $\omega_{tr}^{\text{thigh}}$ is lower than a threshold $\text{th}_5^{sa}$.

These events segment stair ascending in three phases, during which the ankle joint is braked. In the stance phase (FC to FO), the knee joint extends up to the angle $\beta_1^{sa}$ to transfer the user's body upward. In early swing (FO to MF), the knee flexes up to the angle $\beta_2^{sa}$. In late swing (MF to FC), the knee joint is braked to facilitate proper foot placement on the next step.

*3) Stair Descending:* The FSM of stair descending, as shown in Fig. 4(c), decodes two events.

1) *FC*: The vGRF is above a threshold $\text{th}_1^{sd}$.
2) *FO*: Three conditions must be verified within 70 ms. The knee joint is flexed above an angle $\text{th}_2^{sd}$, the standard deviation of the knee joint over five samples $\sigma_{\tau_k}$ is above a threshold $\text{th}_3^{sd}$, and the zero crossing of the angular speed of the shank around the transversal axis $\omega_{tr}^{\text{shank}}$ is detected.

FC and FO segment stair descending into stance and swing. In both phases, the ankle is braked in a neutral position. During stance, the knee joint is commanded by an extension torque $\tau_{\text{des}}$ proportional to the measured knee flexion angle $\theta_k$ and the flexion rate $\dot{\theta}_k$

$$\tau_{\text{des}}(t) = -k_1 \cdot \theta_k(t) - k_2 \cdot \dot{\theta}_k(t) + \tau_0 \tag{4}$$

where $k_1$ and $k_2$ are the stiffness and damping constants, and $\tau_0$ is an offset value that ensures torque continuity. After FO, the knee joint is extended up to the angle $\beta_1^{sd}$.

The ankle joint is locked during stair negotiation to foster shock absorption at FC and improve the perceived stability of the prosthesis in tasks that are typically challenging for people with a transfemoral amputation [17].

*4) Sit/Stand Transitions:* When the user is standing, the BER is in the Both configuration to bear the user's weight. During stand-to-sit, the ankle joint is braked, and the knee is commanded by an extension torque that increases as the user's center of mass moves downward. The torque $\boldsymbol{\tau_{des}}$ is computed as follows:

$$\tau_{\text{des}}(t) = -k_1 \cdot \theta_k(t) - k_2 \cdot \sin(2 \cdot \theta_k(t)) + \tau_0 \tag{5}$$

where $\theta_k$ is the knee joint angle, $k_1$ and $k_2$ are the stiffness constants, and $\tau_0$ ensures the torque continuity during the transition. The first term of the equation is proportional to the measured knee flexion angle, while the sinusoidal term increases the desired torque in the middle of the movement. Once the user is seated, the controller unloads the knee joint by commanding zero torque, and the BER goes in the *Both* configuration. When sitting, the knee joint is not constrained to a particular angle, thus enabling sitting down and standing up from any chair's height.

During sit-to-stand, the ankle joint is braked and the knee joint is controlled along a sigmoidal reference trajectory to reach a fully extended position.

## III. Benchtop Experiments

### A. Characterization of the Position Regulators

The characterization of the PID position regulators was performed in the *Single* configuration. The prosthesis was placed horizontally on the bench without external loads applied at the joints.

Five consecutive steps of 5°, 10°, and 15° were commanded at each joint starting from the 0° position. The step response was characterized by computing the mean and standard deviation of the rise time (i.e., the time to reach 90% of the reference value), settling time (i.e., the time required by the system to reach and remain within ±5% of the reference), and overshoot (i.e., the maximum output value with respect to the reference). In addition, able-bodied gait trajectories were commanded to each prosthetic joint at three speeds (0.4, 0.6, and 0.8 m/s) [42], selected considering that the joints of the SynPro can reach a maximum angular speed of 200°/s [54], [55]. To evaluate the position-tracking performance, we considered the root-mean-square error (RMSE) between the measured and the reference position, and the difference between the maximum reference and measured peak (of flexion and plantarflexion, respectively, for the knee and ankle joints). Mean values and standard deviations were computed over five consecutive repetitions. Finally, the closed-loop system transfer function was estimated by commanding three chirp wave inputs of 10° each, within the frequency range of 0.01–3 Hz. In fact, this range encompasses the typical frequency content of locomotion tasks performed by individuals with transfemoral amputation [4]. The bandwidth of the regulators was computed as the frequency at which either the −3 dB threshold was crossed or the current set by the servo amplifier reached saturation.

The benchtop tests on the position regulators are shown in Fig. 5(a)–(e) for the knee joint and in Fig. 5(f)–(j) for the ankle joint. The metrics computed for the step response and trajectory tracking tests are reported in Table II. Only non-zero standard deviations are reported. The bandwidths of the position regulators were 2.9 Hz for the knee joint and 2.5 Hz for the ankle joint.

### B. Characterization of the Torque Regulators

The PID torque regulators were tuned and characterized in stationary conditions to avoid movements of the joints (i.e., both joints were mechanically blocked). Five steps of 15 and 30 N·m were commanded at each joint in the *Single* configuration. To estimate the closed-loop bandwidth, three chirp wave inputs of 15 N·m were commanded at each joint within the frequency range of 0.01–3 Hz. The benchtop tests on the torque regulators are shown in Fig. 5(k) and (l) for the knee joint and in Fig. 5(m) and (n) for the ankle joint. The metrics computed for the step

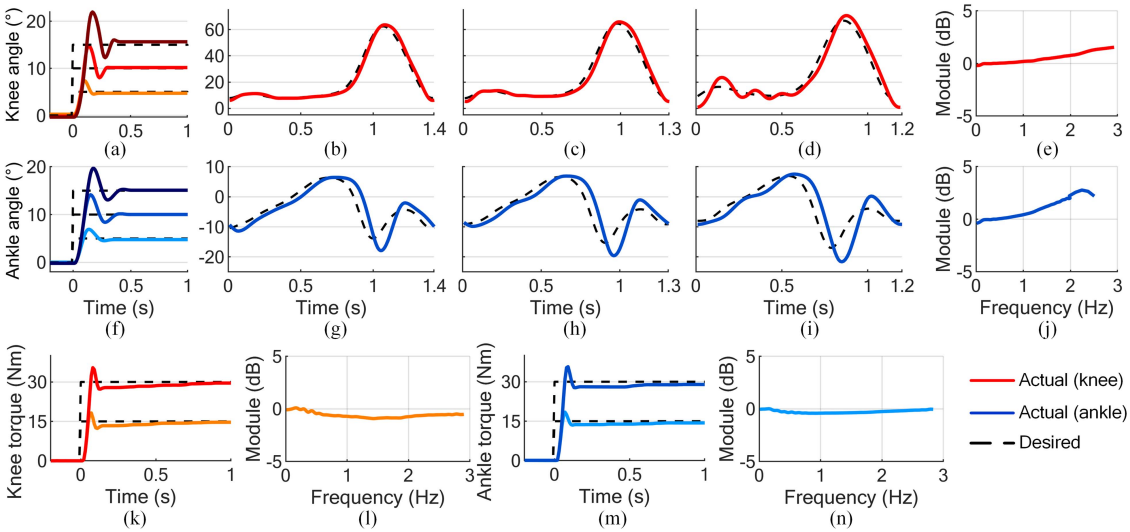


Fig. 5. Benchtop tests' results. Characterization of the closed-loop position regulator of the knee joint: (a) step response; (b) tracking of the able-bodied gait trajectory at 0.4 m/s, (c) 0.6 m/s, and (d) 0.8 m/s; and (e) estimated closed-loop system transfer function. Characterization of the closed-loop position regulator of the ankle joint: (f) step response, (g) tracking of the able-bodied gait trajectory at 0.4 m/s, (h) 0.6 m/s, and (i) 0.8 m/s; and (j) estimated closed-loop system transfer function. Characterization of the closed-loop torque regulator of the knee joint: (k) step response and (l) estimated closed-loop system transfer function. Characterization of the closed-loop torque regulator of the ankle joint: (m) step response and (n) estimated closed-loop system transfer function.

TABLE II
BENCHTOP EXPERIMENTS' RESULTS

| | | Knee joint | | | Ankle joint | | |
|---|---|---|---|---|---|---|---|
| | Step amplitude | **5°** | **10°** | **15°** | **5°** | **10°** | **15°** |
| Step response position | Rise time (ms) | 60 | 90 | 110 | 80 | 90 | 110 |
| | Settling time (ms) | 140 | 260 | 310 | 260 | 330 | 350 |
| | Overshoot (%) | 42.89 ± 0.65 | 49.83 ± 1.05 | 48.86 ± 0.27 | 37.79 ± 0.09 | 43.04 ± 0.24 | 32.67 ± 0.06 |
| | Trajectory speed | **0.4 m/s** | **0.6 m/s** | **0.8 m/s** | **0.4 m/s** | **0.6 m/s** | **0.8 m/s** |
| Trajectory tracking position | RMSE (°) | 2.61 ± 0.01 | 2.96 ± 0.01 | 4.66 ± 0.07 | 2.98 | 3.37 ± 0.01 | 4.28 ± 0.02 |
| | Peak error (°) | 1.18 ± 0.02 | 1.29 ± 0.02 | 3.94 ± 0.27 | 4.09 ± 0.03 | 4.29 ± 0.02 | 4.64 ± 0.03 |
| | Step amplitude | **15 Nm** | | **30 Nm** | **15 Nm** | | **30 Nm** |
| Step response torque | Rise time (ms) | 40 | | 60 | 50 | | 60 |
| | Settling time (ms) | 540 ± 50 | | 470 ± 60 | 640 ± 50 | | 530 ± 40 |
| | Overshoot (%) | 21.34 ± 0.47 | | 20.51 ± 1.84 | 29.84 ± 4.02 | | 23.16 ± 0.14 |

response are reported in Table II. Both bandwidths of the torque regulators exceed 3 Hz, as the −3 dB crossing was not observed for either joint within the tested range of frequencies.

### C. Characterization of the Engagement of the Brakes

The performance of the BER was characterized through bench tests aimed at evaluating:

1) the dynamics of brake engagement;
2) the effect of introducing latency when switching the brakes' engagement in the *Single* configuration;
3) the proportional brake engagement in the *None* configuration.

During these tests, the prosthesis was positioned horizontally on the bench and the joints were controlled in position. The amplitude and duration of the reference trajectories were chosen to achieve joint speeds in the range of 100–200°/s, which corresponds to the angular speed of the knee and ankle joints during walking at 0.6 m/s [54]. To evaluate the dynamics of brake engagement, a sigmoidal curve with an amplitude of 20° and a duration of 400 ms was commanded to one joint while the other joint was braked. The joint was braked when it reached the 10° position (at time $t_{BE}$). This test was repeated five times. The time required for the brake to decelerate the output joint below 10°/s was 130 ms for the knee joint ($\Delta_k$) and 200 ms for the ankle joint ($\Delta_a$). The joint displacement after being braked was 4.22 ± 0.20° for the knee joint ($\delta_k$) and 15.21 ± 0.27° for the ankle joint ($\delta_a$) [see Fig. 6(a) and (b)].

To assess the functionality of the BER in the *Single* configuration, a sinewave with an amplitude of 20° and a frequency of 0.8 Hz was commanded to the knee joint while the ankle joint was braked. After three periods, the control was switched to the ankle joint, and the knee joint was braked [see Fig. 6(c)]. This sequence was repeated in two conditions: instantaneous switching (referred to as BER off) and switching with a time

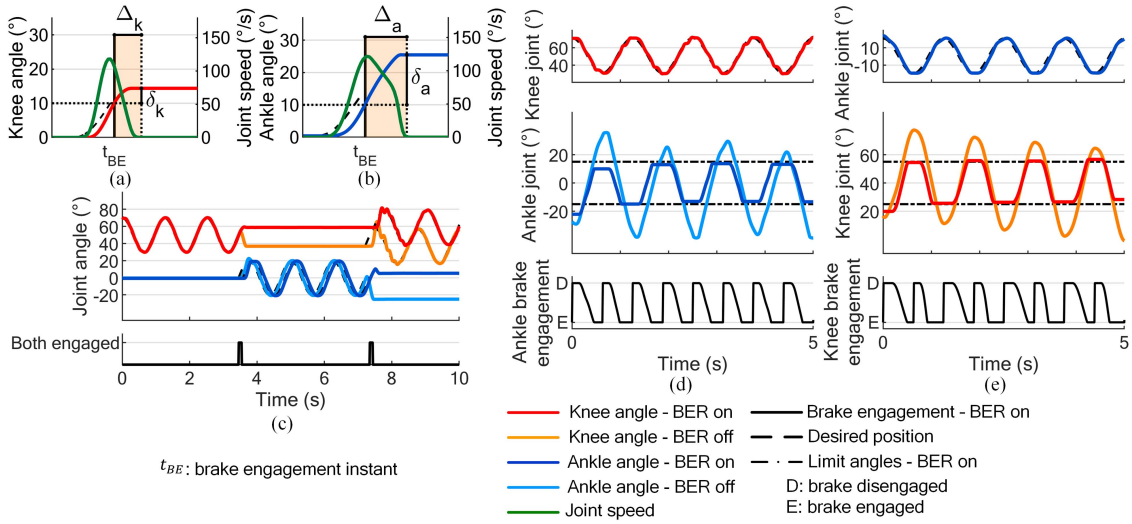


Fig. 6. Characterization of the brakes' engagement. Instantaneous engagement of the (a) knee brake and (b) ankle brake. (c) Switching of the brakes' engagement. The lower subplot displays the 130 ms in which the brakes are both engaged. (d) Proportional engagement of the ankle brake while the knee joint is tracking a sinewave. (e) Proportional engagement of the knee brake while the ankle joint is tracking a sinewave. Tests (c)–(e) were performed both with the BER disabled (off) and enabled (on).

window in which both brakes are engaged (referred to as BER on) [as shown in Fig. 6(c)]. In the BER off condition, the joint displacement was 14.2° for the knee joint and 25.1° for the ankle joint. By introducing the time window of 130 ms (BER on), these values were reduced to 7.8° for the knee joint and 4.4° for the ankle joint.

To assess the functionality of the BER in the *None* configuration, the following test was performed with both the BER off and the BER on: a sinewave with an amplitude of 20° and a frequency of 0.8 Hz was commanded to one joint while the opposite joint was free to move. Due to the transmission stages, the noncontrolled joint tended to drift toward lower angular values: the ankle joint drifted at a rate of 1.8°/s, and the knee joint at a rate of 1.7°/s [see the orange and light blue curves in Fig. 6(d) and (e)]. By enabling the BER, the movement of the noncontrolled joint was effectively constrained between software-set thresholds of −15° and −15° for the ankle joint and 25° and 55° for the knee joint [see the red and blue curves in Fig. 6(d) and (e)]. The timing of brake engagement varied with the velocity at which the noncontrolled joint approached the thresholds [in accordance with (3)]. Therefore, the tendency to approach the lower threshold more rapidly resulted in a "long–short" braking pattern for the knee joint [see Fig. 6(e)]. Since during the test, the ankle joint exhibited lower velocities compared with the knee joint; the pattern is less pronounced in Fig. 6(d).

## IV. Experiments With Transfemoral Amputees

A multicenter experimental protocol was developed to demonstrate the feasibility of the SynPro in the main locomotion tasks: level-ground walking, stair ascending and descending, and sit/stand transitions. The protocol was approved by the Ethics Committees of Area Vasta Toscana Centro (study number 16677) and Area Vasta Emilia Centro (study number 19168), and written informed consent was obtained from each participant prior to the sessions. The experimental activities were conducted at two locations: IRCCS Fondazione Don Carlo Gnocchi, Florence, Italy (FDG) and Centro Protesi Inail, Vigorso di Budrio, Bologna, Italy. Three individuals with above-knee amputation were recruited for the study (see Table III). All subjects were fitted with the prosthesis by a certified prosthetist and instructed to complete the tasks by a licensed therapist, while researchers were operating the prosthesis and monitoring its correct functioning throughout the experiments. Handrails were provided to the subjects for support during all tasks. Prior to the experiments, the default control parameters of the SynPro were tuned on a nonamputee subject wearing a knee-bend adaptor to use the prosthesis. A subset of the parameters was further fine-tuned for each subject during a 30-min training phase before each recording session.

The mean and standard deviation of the position and torque profiles of the knee and ankle joints are presented for each subject in Fig. 7, along with able-bodied ranges computed from [39] and [56]. These ranges were extracted considering a walking speed of 0.5 m/s, which is comparable to the self-selected speed of the subjects wearing the SynPro, and a step height of 10.2 cm for stair negotiation. The strides were segmented based on FC, and their duration was normalized as a percentage of stride time. The measured joint torques were normalized by the subjects' weights. Data for each participant are shown separately: yellow and light blue curves represent subject 1, orange and blue curves represent subject 2, and red and dark blue curves represent subject 3.

### A. Walking

Each participant completed treadmill walking at a self-selected speed (0.42 m/s for subjects 1 and 2, and 0.47 m/s for subject 3). During the task, the following subset of parameters

TABLE III
ENROLLED SUBJECTS

| ID | Gender | Age | Weight | Height | Amputation type | Years from amputation | Used prosthesis | Amputation side | K-score |
|---|---|---|---|---|---|---|---|---|---|
| 1 | Male | 74 | 62 kg | 179 cm | Traumatic | 19 | C-Leg | Right | K3 |
| 2 | Male | 52 | 82 kg | 172 cm | Traumatic | 15 | Genium X3 | Left | K3 |
| 3 | Male | 54 | 73 kg | 180 cm | Traumatic | 13 | Genium X3 | Right | K4 |

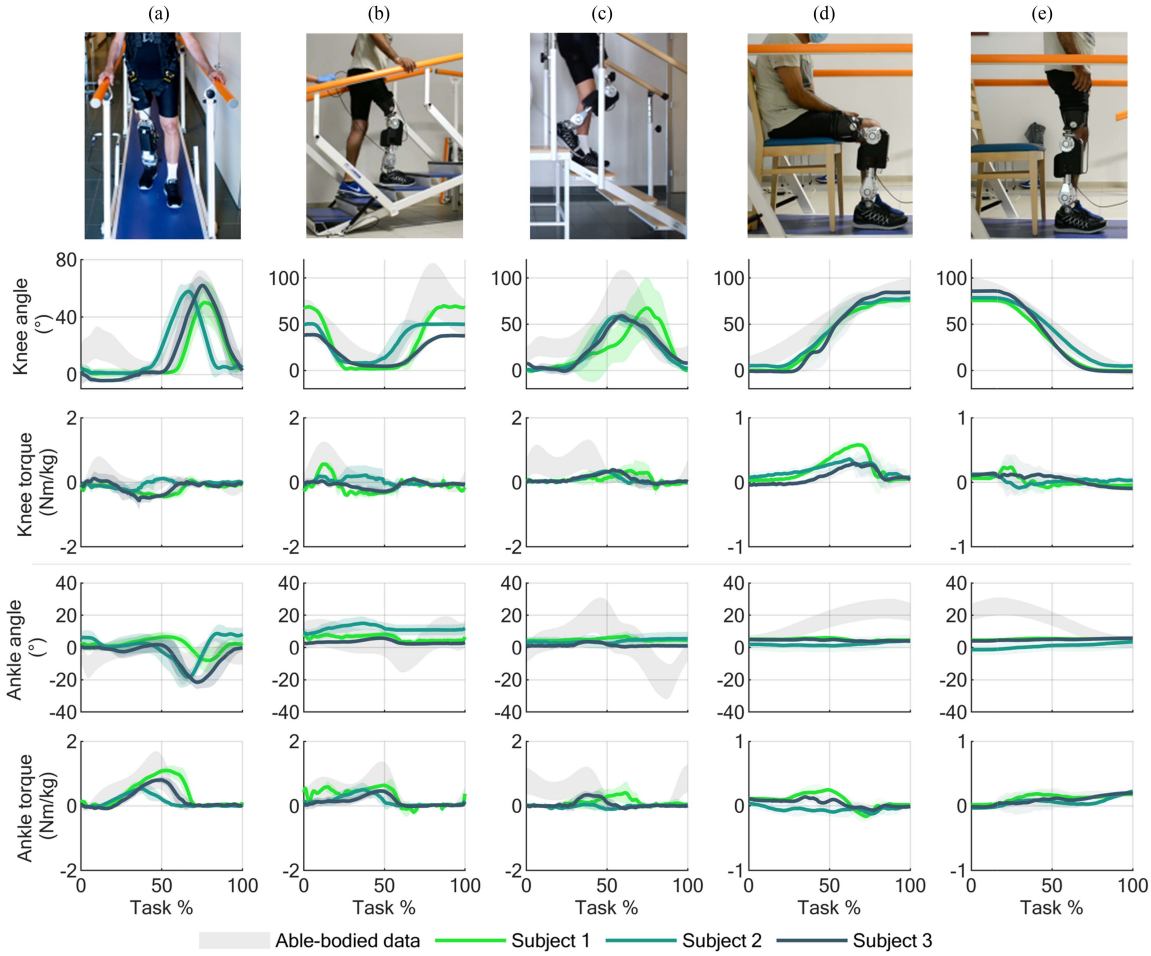


Fig. 7. Position and torque profiles of the knee and ankle joints for (a) overground walking, (b) stair ascending, (c) stair descending, (d) stand-to-sit, and (e) sit-to-stand. Solid lines represent average curves, while shaded areas of the same color represent their respective standard deviations. Shaded gray areas are the standard deviations of able-bodied data, adapted from [39] and [56].

was tuned for each subject: the thresholds for the center of pressure to detect HO ($\text{th}_6^{wk}$, $\text{th}_7^{wk}$), the desired knee angle during late stance ($\beta_2^{wk}$), and the duration of the knee position references in late stance and late swing. Afterward, each subject was asked to walk at a comfortable pace over a 6 m corridor with the set of control parameters tuned during treadmill walking. The average walking profiles, as shown in Fig. 7(a), were computed over the strides of two consecutive corridors. Kinematic and kinetic metrics for level-ground walking are reported in Table IV. The maximum knee flexion angle during swing was within normative ranges for all subjects [39] and occurred at around 70% of the gait cycle, allowing swing clearance. During swing, the kinematic coupling enabled the dorsiflexion of the ankle joint, while the power actuator controlled the extension of the knee (see the peak ankle plantarflexion angles in Table IV). The average ankle peak torque and power were within normative ranges for subjects 1 and 3, and slightly below for subject 2.

### B. Stair Ascent and Stair Descent

During stair negotiation tasks, each subject was asked to ascend and descend a staircase at a self-selected pace. The staircases used for this task differed in the two facilities: a staircase with four steps (each 16 cm high) was available in FDG, while Centro Protesi Inail was equipped with a staircase with five steps (each 9.5 cm high). Prior to data recording, the following control parameters for stair ascending were fine-tuned for each subject: the thresholds to detect FC and FO based on the vertical ground reaction force ($\text{th}_1^{sa}$ and $\text{th}_2^{sa}$) and the desired knee flexion angle ($\beta_2^{sa}$). Control parameters for stair descending did not require further tuning. The average stair ascend/descend profiles

TABLE IV
JOINT METRICS DURING WALKING AND STAIR NEGOTIATION

| | | Subject 1 | Subject 2 | Subject 3 |
|---|---|---|---|---|
| Level-ground walking | Peak knee flexion (°) | 50 | 58 | 62 |
| | Peak ankle plantarflexion (°) | 8 | 18.3 | 21.5 |
| | Knee flexion torque (Nm/kg) | 0.44 | 0.27 | 0.57 |
| | Ankle plantarflexion torque (Nm/kg) | 1.1 | 0.53 | 0.8 |
| Stair ascent | Peak knee flexion (°) | 70 | 50.4 | 38.6 |
| | Peak knee power (W/kg) | 1.46 | 0.37 | 0.11 |
| | Ankle plantarflexion torque (Nm/kg) | 0.64 | 0.5 | 0.46 |
| Stair descent | Peak knee flexion (°) | 67.4 | 58.1 | 59 |
| | Peak knee power (W/kg) | 0.91 | 0.82 | 1.07 |
| | Ankle plantarflexion torque (Nm/kg) | 0.36 | 0.34 | 0.39 |

for each subject were produced by computing the mean over five steps [see Fig. 7(b) and (c)]. Kinematic and kinetic metrics for stair negotiation are reported in Table IV. The active knee flexion enabled each subject to climb the stairs in a step-over-step manner. Both in stair descending and ascending, the ankle joint was braked. Nonetheless, the elasticity at the ankle joint allowed the exertion of plantarflexion torques up to 0.64 N·m/kg in stair ascending and 0.39 N·m/kg in stair descending.

### C. Sit/Stand Transitions

Each subject was asked to sit down and stand up from a chair. Before data recording, the stiffness constant $k_1$ and the duration of the sigmoidal reference for the knee position were tuned based on individual preferences. For each subject, the position and torque profiles, as reported in Fig. 7(d) and (e), were averaged over five transitions. During stand-to-sit transitions, the average knee peak torque was 0.58 N·m/kg for subject 1, 0.36 N·m/kg for subject 2, and 0.29 N·m/kg for subject 3. In sit-to-stand transitions, the knee torque had average peaks of 0.24 N·m/kg, 0.13 N·m/kg, and 0.14 N·m/kg for subjects 1, 2, and 3, respectively.

## V. DISCUSSION

In this article, we presented the MOTU Transfemoral SynPro, a battery-powered device equipped with a differential mechanism to distribute the power generated by a single power actuator to both the knee and ankle joints. This design principle aligns with the varying power demands of the two joints across different locomotion tasks and gait phases. In fact, the power required to actuate the combination of the knee and ankle joints is lower than that needed for separate actuation of each joint. Beyond potentially reducing power consumption, underactuation also eliminates the need for mechanical and electrical components associated with a second power actuator. While our prototype employs a single 200 W actuator to power both the knee and ankle joints, most transfemoral prostheses utilize separate actuators with a combined power higher than 200 W [23], [57], [58].

### A. Feasibility of a Knee–Ankle Underactuated Prosthesis

Benchtop tests demonstrated that the actuation unit can accurately control the position and the torque of each joint, with controllers' bandwidths above 2.5 Hz. While able-bodied human locomotion encompasses frequency content up to 6 Hz, the recorded control bandwidths are suitable for typical locomotion tasks at comfortable self-selected speeds and cadences specific to people with transfemoral amputations, who constitute our target population [4], [59]. In fact, the SynPro successfully tracked gait trajectories up to 0.6 m/s, exhibiting low RMSE. At 0.8 m/s, the main discrepancies with the desired trajectories were a slight delay and overshooting of the peak angles. Nonetheless, the joints remained within the physiological range of movement, without reaching the mechanical end stops. The benchtop tests demonstrated the capability of the BER to manage the braking dynamics [see Fig. 6(c)] and the synergic actuation of the knee and ankle joints by keeping the noncontrolled joint within software-set thresholds [see Fig. 6(d) and (e)].

Potential variations in the performance of the position controllers and the braking system under loaded conditions did not significantly affect the capability of the device to follow biomechanical trajectories. This was evidenced by the experimental evaluation conducted with three subjects with a transfemoral amputation, which demonstrated the compatibility of knee–ankle underactuation with the main locomotion tasks: the differential mechanism enabled the synergic movement of the knee and ankle joints during late stance and late swing, and the braking system managed the synergy between the two joints and enabled the execution of stair negotiation and sit/stand transitions by conveying motor power solely to the knee joint. Most control parameters and gait segmentation thresholds were tuned beforehand on a healthy subject and were left unchanged. By manually tuning a few parameters, the prosthesis could adapt to different cadences and step heights.

Walking tests showed that all participants were able to walk overground with the SynPro at a comfortable pace, with joints' kinematics resembling able-bodied biomechanics. In level-ground walking, the power actuator controlled the movement of the ankle joint only during early stance. During the other walking phases, the BER kept the synergic movement of the ankle joint within physiological ranges for all subjects [39]. Moreover, the coupling between the two joints enabled a peak ankle plantarflexion up to 21.5° during late stance. Due to different controller parametrizations, we observed that the maximum ankle plantarflexion reached during swing differed across subjects. For example, subject 1 preferred a lower maximum knee flexion during a late stance. Since, in this phase, the ankle movement is coupled to the knee movement, this lowered the maximum plantarflexion angle reached by the ankle in late stance. The low familiarity with the device may have increased the use of handrails during the locomotion tasks. This could have

contributed to the torque and power estimates being lower than nonamputee references [60]. Moreover, when the prosthesis was in contact with the ground, the elastic foot absorbed a part of the energy that would, otherwise, have compressed the elastic elements at the ankle, thus lowering the torque recorded at the joint.

In stair negotiation tasks, the participants benefited from the actuated knee joint to ascend and descend stairs in a step-over-step manner. The prosthesis demonstrated adaptability to varying step heights by generating higher knee power to climb higher steps, as evidenced by data collected during the trials with subject 1 (see the peak knee power during stair ascent in Table IV). At the end of each stair descent gait cycle, the knee joint was fully extended to enhance the perceived stability of the prosthesis at heel strike. Conversely, in able-bodied kinematics, the knee is typically flexed at heel strike. This different knee positioning resulted in lower recorded torques at the beginning of stair descent compared with able-bodied data.

Although the ankle joint was not actuated in stair negotiation tasks, the series elastic element and the elastic foot enabled the absorption and release of energy during stance and the beginning of swing. Nonetheless, having the ankle locked during these tasks limited the torque—thus the power—exerted at the joint.

The powered knee extension enabled each subject to stand up from a chair, and the proportional torque commanded at the knee joint allowed for a controlled sitting down.

### B. Limitations

The SynPro is a proof-of-concept prototype for the design principle of knee–ankle underactuation. While experiments with subjects with transfemoral amputations showed the capability of the device to replicate the kinematics of the knee and ankle joints in the main locomotion tasks, there are some limitations to consider. The weight of the device, despite being comparable with existing prototypes [23], [57], [61], is the main obstacle for its usability. A substantial portion of the SynPro weight comes from the multiple transmission stages used to deliver the power of the actuation unit to the two joints and the elastic elements. In fact, the SynPro is equipped with series elasticity at both prosthetic joints, while in the transfemoral prosthesis series, the elastic elements are often used only at the knee joint [19], [20]. While the elastic elements at the ankle joint enable a force-sensing architecture and promote compliance, their removal would reduce the prosthesis mass by over 0.3 kg. Additionally, future design iterations will focus on reducing the weight and volume attributed to the transmission stages, the sensors, and the control electronics. For instance, a future iteration will explore the potential replacement of servomotors and disc brakes with electromechanical clutches.

The braking system also generates delays and introduces frictions at the outputs of the differential (i.e., before the transmission chain to the joints). The elastic elements enabled torque sensing after the transmission stages of the joints, resulting in a closed-loop torque controller that inherently compensates for losses within the transmission chain. Nonetheless, the braking system and the lengthy transmission chain currently limit the utilization of the SynPro in locomotion tasks at low-to-average speeds.

While the control strategy of the SynPro currently exploits the knee–ankle kinematic synergies during late stance and swing, further analysis should focus on exploring different actuation strategies to take advantage of the accurate torque feedback at the prosthetic joints and decrease the number of control parameters. For example, adaptive algorithms could be employed for the online tuning of control parameters (e.g., the knee flexion during the swing) or for automatic locomotion-mode recognition based on volitional data coming from the residual leg of the user [62], [63].

## VI. Conclusion

In this article, we presented the mechatronic design of the SynPro, an underactuated transfemoral prosthesis equipped with a differential mechanism to distribute the power of a single motor to the knee and ankle joints. Benchtop tests demonstrated the capability of the actuation unit to drive the prosthetic joints along physiological gait trajectories. Additionally, the braking system was able to effectively manage the joints' movement during synergistic actuation and enabled the execution of tasks that did not require synergic actuation. The compatibility of knee–ankle underactuation with the main locomotion tasks was further confirmed by experiments with three subjects with above-knee amputations using the prosthesis to perform overground walking, stair ascending and descending, and sit/stand transitions.

While the primary aim of the present study was to evaluate the feasibility of a knee–ankle underactuated design, the experiments provided insights into the requirements for developing a lighter and more efficient prototype exploiting this principle. Therefore, future design iterations will focus on revising the prosthesis' mechatronic design to reduce weight and streamline the transmission chain, thereby enhancing the efficiency of power distribution to the knee and ankle joints.

We advocate for the deeper exploration of underactuation in transfemoral prostheses due to its potential benefits in optimizing weight distribution, power efficiency, and reducing encumbrance while maintaining two powered joints. This approach aligns with the distinct power demands of the knee and ankle joints during different phases of locomotion, suggesting a promising direction for further advancement in prosthetic design.

## References

[1] M. Narres et al., "Incidence of lower extremity amputations in the diabetic compared with the non-diabetic population: A systematic review," *PLoS One*, vol. 12, no. 8, Aug. 2017, Art. no. e0182081, doi: 10.1371/journal.pone.0182081.

[2] F. L. Lombardo, M. Maggini, A. De Bellis, G. Seghieri, and R. Anichini, "Lower extremity amputations in persons with and without diabetes in Italy: 2001–2010," *PLoS One*, vol. 9, no. 1, Jan. 2014, Art. no. e86405, doi: 10.1371/journal.pone.0086405.

[3] K. Ziegler-Graham, E. J. MacKenzie, P. L. Ephraim, T. G. Travison, and R. Brookmeyer, "Estimating the prevalence of limb loss in the United States: 2005 to 2050," *Arch. Phys. Med. Rehabil.*, vol. 89, no. 3, pp. 422–429, Mar. 2008, doi: 10.1016/j.apmr.2007.11.005.

[4] L. Guirao et al., "Distance and speed of walking in individuals with trans-femoral amputation fitted with a distal weight-bearing implant," *Orthopaedics Traumatol., Surg. Res.*, vol. 104, no. 6, pp. 929–933, Oct. 2018, doi: 10.1016/j.otsr.2018.04.011.

[5] S. W. Hunter, F. Batchelor, K. D. Hill, A.-M. Hill, S. Mackintosh, and M. Payne, "Risk factors for falls in people with a lower limb amputation: A systematic review," *PM&R*, vol. 9, no. 2, pp. 170–180, Feb. 2017, doi: 10.1016/j.pmrj.2016.07.531.

[6] R. L. Waters, J. Perry, D. Antonelli, and H. Hislop, "Energy cost of walking of amputees: The influence of level of amputation," *J. Bone Joint Surg. Amer.*, vol. 58, no. 1, pp. 42–46, Jan. 1976.

[7] L. Nolan, A. Wit, K. Dudziñski, A. Lees, M. Lake, and M. Wychowañski, "Adjustments in gait symmetry with walking speed in trans-femoral and trans-tibial amputees," *Gait Posture*, vol. 17, no. 2, pp. 142–151, Apr. 2003, doi: 10.1016/S0966-6362(02)00066-8.

[8] M. J. Miller, J. Jones, C. B. Anderson, and C. L. Christiansen, "Factors influencing participation in physical activity after dysvascular amputation: A qualitative meta-synthesis," *Disabil. Rehabil.*, vol. 41, no. 26, pp. 3141–3150, Dec. 2019, doi: 10.1080/09638288.2018.1492031.

[9] A. L. Mayo et al., "Self-reported health condition severity and ambulation status postmajor dysvascular limb loss," *Prosthetics Orthotics Int.*, vol. 46, no. 3, pp. 239–245, Jun. 2022, doi: 10.1097/PXR.0000000000000106.

[10] J. Bernatchez, A. L. Mayo, and A. Kayssi, "The epidemiology of lower extremity amputations, strategies for amputation prevention, and the importance of patient-centered care," *Seminars Vasc. Surg.*, vol. 34, no. 1, pp. 54–58, Mar. 2021, doi: https://doi.org/10.1053/j.semvascsurg.2021.02.011.

[11] T. Lenzi and L. Hargrove, "User-adaptive control of robotic lower limb prostheses," in *The Encyclopedia of Medical Robotics*. Singapore: World Scientific, 2018, pp. 89–110, doi: 10.1142/9789813232327_0004.

[12] L. Nolan and A. Lees, "The functional demands on the intact limb during walking for active transfemoral and transtibial amputees," *Prosthetics Orthotics Int.*, vol. 24, no. 2, pp. 117–125, Aug. 2000, doi: 10.1080/03093640008726534.

[13] B. Sivapuratharasu, A. M. J. Bull, and A. H. McGregor, "Understanding low back pain in traumatic lower limb amputees: A systematic review," *Arch. Rehabil. Res. Clin. Transl.*, vol. 1, no. 1/2, Jun. 2019, Art. no. 100007, doi: 10.1016/j.arrct.2019.100007.

[14] R. Gailey, "Review of secondary physical conditions associated with lower-limb amputation and long-term prosthesis use," *J. Rehabil. Res. Develop.*, vol. 45, no. 1, pp. 15–30, Dec. 2008, doi: 10.1682/JRRD.2006.11.0147.

[15] B. E. Lawson, H. A. Varol, A. Huff, E. Erdemir, and M. Goldfarb, "Control of stair ascent and descent with a powered transfemoral prosthesis," *IEEE Trans. Neural Syst. Rehabil. Eng.*, vol. 21, no. 3, pp. 466–473, May 2013, doi: 10.1109/TNSRE.2012.2225640.

[16] S. Culver, H. Bartlett, A. Shultz, and M. Goldfarb, "A stair ascent and descent controller for a powered ankle prosthesis," *IEEE Trans. Neural Syst. Rehabil. Eng.*, vol. 26, no. 5, pp. 993–1002, May 2018, doi: 10.1109/TNSRE.2018.2819508.

[17] G. R. Hunt, S. Hood, L. Gabert, and T. Lenzi, "Effect of increasing assistance from a powered prosthesis on weight-bearing symmetry, effort, and speed during stand-up in individuals with above-knee amputation," *IEEE Trans. Neural Syst. Rehabil. Eng.*, vol. 31, pp. 11–21, 2023, doi: 10.1109/TNSRE.2022.3214806.

[18] A. Mazzarini et al., "A low-power ankle-foot prosthesis for push-off enhancement," *Wearable Technol.*, vol. 4, 2023, Art. no. e18, doi: 10.1017/wtc.2023.13.

[19] L. Flynn et al., "The challenges and achievements of experimental implementation of an active transfemoral prosthesis based on biological quasi-stiffness: The CYBERLEGs beta-prosthesis," *Front. Neurorobot.*, vol. 12, Dec. 2018, Art. no. 80, doi: 10.3389/fnbot.2018.00080.

[20] A. F. Azocar, L. M. Mooney, J.-F. Duval, A. M. Simon, L. J. Hargrove, and E. J. Rouse, "Design and clinical implementation of an open-source bionic leg," *Nature Biomed. Eng.*, vol. 4, no. 10, pp. 941–953, Oct. 2020, doi: 10.1038/s41551-020-00619-3.

[21] B. E. Lawson, J. Mitchell, D. Truex, A. Shultz, E. Ledoux, and M. Goldfarb, "A robotic leg prosthesis: Design, control, and implementation," *IEEE Robot. Autom. Mag.*, vol. 21, no. 4, pp. 70–81, Dec. 2014, doi: 10.1109/MRA.2014.2360303.

[22] E. J. Rouse, L. M. Mooney, and H. M. Herr, "Clutchable series-elastic actuator: Implications for prosthetic knee design," *Int. J. Robot. Res.*, vol. 33, no. 13, pp. 1611–1625, Nov. 2014, doi: 10.1177/0278364914545673.

[23] T. Elery, S. Rezazadeh, C. Nesler, and R. D. Gregg, "Design and validation of a powered knee–ankle prosthesis with high-torque, low-impedance actuators," *IEEE Trans. Robot.*, vol. 36, no. 6, pp. 1649–1668, Dec. 2020, doi: 10.1109/TRO.2020.3005533.

[24] T. Lenzi, M. Cempini, L. Hargrove, and T. Kuiken, "Design, development, and testing of a lightweight hybrid robotic knee prosthesis," *Int. J. Robot. Res.*, vol. 37, no. 8, pp. 953–976, Jul. 2018, doi: 10.1177/0278364918785993.

[25] J. T. Lee, H. L. Bartlett, and M. Goldfarb, "Design of a semipowered stance-control swing-assist transfemoral prosthesis," *IEEE/ASME Trans. Mechatron.*, vol. 25, no. 1, pp. 175–184, Feb. 2020, doi: 10.1109/TMECH.2019.2952084.

[26] M. Cempini, L. J. Hargrove, and T. Lenzi, "Design, development, and bench-top testing of a powered polycentric ankle prosthesis," in *Proc. IEEE/RSJ Int. Conf. Intell. Robots Syst.*, Vancouver, BC, Canada, 2017, pp. 1064–1069, doi: 10.1109/IROS.2017.8202276.

[27] M. Tran, L. Gabert, M. Cempini, and T. Lenzi, "A lightweight, efficient fully powered knee prosthesis with actively variable transmission," *IEEE Robot. Autom. Lett.*, vol. 4, no. 2, pp. 1186–1193, Apr. 2019, doi: 10.1109/LRA.2019.2892204.

[28] M. C. Carrozza, G. Cappiello, S. Micera, B. B. Edin, L. Beccai, and C. Cipriani, "Design of a cybernetic hand for perception and action," *Biol. Cybern.*, vol. 95, no. 6, Dec. 2006, Art. no. 629, doi: 10.1007/s00422-006-0124-2.

[29] M. Controzzi, F. Clemente, D. Barone, A. Ghionzoli, and C. Cipriani, "The SSSA-MyHand: A dexterous lightweight myoelectric hand prosthesis," *IEEE Trans. Neural Syst. Rehabil. Eng.*, vol. 25, no. 5, pp. 459–468, May 2017, doi: 10.1109/TNSRE.2016.2578980.

[30] M. Laffranchi et al., "The Hannes hand prosthesis replicates the key biological properties of the human hand," *Sci. Robot.*, vol. 5, no. 46, Sep. 2020, Art. no. eabb0467, doi: 10.1126/scirobotics.abb0467.

[31] E. Capotorti et al., "A novel torque-controlled hand exoskeleton to decode hand movements combining SEMG and fingers kinematics: A feasibility study," *IEEE Robot. Autom. Lett.*, vol. 7, no. 1, pp. 239–246, Jan. 2022, doi: 10.1109/LRA.2021.3111412.

[32] H. K. Ko, S. W. Lee, D. H. Koo, I. Lee, and D. J. Hyun, "Waist-assistive exoskeleton powered by a singular actuation mechanism for prevention of back-injury," *Robot. Auton. Syst.*, vol. 107, pp. 1–9, Sep. 2018, doi: 10.1016/j.robot.2018.05.008.

[33] F. Lanotte et al., "Design and characterization of a multi-joint underactuated low-back exoskeleton for lifting tasks," in *Proc. IEEE 8th RAS/EMBS Int. Conf. Biomed. Robot. Biomechatron.*, New York, NY, USA, 2020, pp. 1146–1151, doi: 10.1109/BioRob49111.2020.9224370.

[34] N. A. Bianco, P. W. Franks, J. L. Hicks, and S. L. Delp, "Coupled exoskeleton assistance simplifies control and maintains metabolic benefits: A simulation study," *PLoS One*, vol. 17, no. 1, Jan. 2022, Art. no. e0261318, doi: 10.1371/journal.pone.0261318.

[35] K. Shimada and T. Takenaka, "Motion assist device," U.S. Patent 2016/0310344A1, Oct. 27, 2016.

[36] L. Gabert, M. Tran, and T. Lenzi, "Design of an underactuated powered ankle and toe prosthesis," in *Proc. 43rd Annu. Int. Conf. IEEE Eng. Med. Biol. Soc.*, Mexico, 2021, pp. 4920–4923, doi: 10.1109/EMBC46164.2021.9629842.

[37] S. Hood, S. Creveling, L. Gabert, M. Tran, and T. Lenzi, "Powered knee and ankle prostheses enable natural ambulation on level ground and stairs for individuals with bilateral above-knee amputation: A case study," *Sci. Rep.*, vol. 12, no. 1, Sep. 2022, Art. no. 15465, doi: 10.1038/s41598-022-19701-8.

[38] J. W. Kwon, S. M. Son, and N. K. Lee, "Changes of kinematic parameters of lower extremities with gait speed: A 3D motion analysis study," *J. Phys. Ther. Sci.*, vol. 27, no. 2, pp. 477–479, 2015, doi: 10.1589/jpts.27.477.

[39] J. Camargo, A. Ramanathan, W. Flanagan, and A. Young, "A comprehensive, open-source dataset of lower limb biomechanics in multiple conditions of stairs, ramps, and level-ground ambulation and transitions," *J. Biomech.*, vol. 119, Apr. 2021, Art. no. 110320, doi: 10.1016/j.jbiomech.2021.110320.

[40] C. Lee, S. Kwak, J. Kwak, and S. Oh, "Generalization of series elastic actuator configurations and dynamic behavior comparison," *Actuators*, vol. 6, no. 3, Aug. 2017, Art. no. 26, doi: 10.3390/act6030026.

[41] F. Lacquaniti, Y. P. Ivanenko, and M. Zago, "Patterned control of human locomotion: Control of human locomotion," *J. Physiol.*, vol. 590, no. 10, pp. 2189–2199, May 2012, doi: 10.1113/jphysiol.2011.215137.

[42] D. A. Winter, "Kinematic and kinetic patterns in human gait: Variability and compensating effects," *Hum. Movement Sci.*, vol. 3, no. 1/2, pp. 51–76, Mar. 1984, doi: 10.1016/0167-9457(84)90005-8.

[43] B. J. McFadyen and D. A. Winter, "An integrated biomechanical analysis of normal stair ascent and descent," *J. Biomech.*, vol. 21, no. 9, pp. 733–744, Jan. 1988, doi: 10.1016/0021-9290(88)90282-5.

[44] G. A. Pratt and M. M. Williamson, "Series elastic actuators," in *Proc. IEEE/RSJ Int. Conf. Intell. Robots Syst. Hum. Robot Interaction Cooperative Robots*, Pittsburgh, PA, USA, 1995, pp. 399–406, doi: 10.1109/IROS.1995.525827.

[45] A. Baldoni, S. Crea, and N. Vitiello, "Wearable active robot for body joints in series," U.S. Patent 2022/0023131 A1, Jan. 27, 2022.

[46] A. Baldoni, M. Fantozzi, and N. Vitiello, "Planar torsional spring," U.S. Patent 2022/0003292 A1, Jan. 6, 2022.

[47] K. Shamaei, G. S. Sawicki, and A. M. Dollar, "Estimation of quasi-stiffness of the human knee in the stance phase of walking," *PLoS One*, vol. 8, no. 3, Mar. 2013, Art. no. e59993, doi: 10.1371/journal.pone.0059993.

[48] Z. Safaeepour, A. Esteki, F. T. Ghomshe, and N. A. Abu Osman, "Quantitative analysis of human ankle characteristics at different gait phases and speeds for utilizing in ankle-foot prosthetic design," *BioMed. Eng. OnLine*, vol. 13, no. 1, 2014, Art. no. 19, doi: 10.1186/1475-925X-13-19.

[49] E. Martini et al., "Pressure-sensitive insoles for real-time gait-related applications," *Sensors*, vol. 20, no. 5, Mar. 2020, Art. no. 1448, doi: 10.3390/s20051448.

[50] T. Fiumalbi et al., "A multimodal sensory apparatus for robotic prosthetic feet combining optoelectronic pressure transducers and IMU," *Sensors*, vol. 22, no. 5, Feb. 2022, Art. no. 1731, doi: 10.3390/s22051731.

[51] S. M. M. de Rossi, T. Lenzi, N. Vitiello, A. Persichetti, F. Giovacchini, and M. C. Carrozza, "Structure of a sensorized mat," WO Patent 2013/027145 A2, Feb. 28, 2013.

[52] E. Martini, A. Baldoni, N. Vitiello, S. Crea, T. Fiumalbi, and F. Dell'Agnello, "Method for optimizing the arrangement of pressure sensors and device obtained by this method," WO Patent 2021/084427 A1, May 6, 2021.

[53] R. Pearce and G. B. Yundt, "Safe torque off over network wiring," WO Patent 2013/028270 A1, Feb. 28, 2013.

[54] B. F. Mentiplay, M. Banky, R. A. Clark, M. B. Kahn, and G. Williams, "Lower limb angular velocity during walking at various speeds," *Gait Posture*, vol. 65, pp. 190–196, Sep. 2018, doi: 10.1016/j.gaitpost.2018.06.162.

[55] V. Monaco, G. Galardi, M. Coscia, D. Martelli, and S. Micera, "Design and evaluation of NEUROBike: A neurorehabilitative platform for bedridden post-stroke patients," *IEEE Trans. Neural Syst. Rehabil. Eng.*, vol. 20, no. 6, pp. 845–852, Nov. 2012, doi: 10.1109/TNSRE.2012.2212914.

[56] E. Reznick, K. R. Embry, R. Neuman, E. Bolívar-Nieto, N. P. Fey, and R. D. Gregg, "Lower-limb kinematics and kinetics during continuously varying human locomotion," *Sci. Data*, vol. 8, no. 1, Oct. 2021, Art. no. 282, doi: 10.1038/s41597-021-01057-9.

[57] N. Thatte, H. Duan, and H. Geyer, "A method for online optimization of lower limb assistive devices with high dimensional parameter spaces," in *Proc. IEEE Int. Conf. Robot. Autom.*, Brisbane, QLD, Australia, 2018, pp. 5380–5385, doi: 10.1109/ICRA.2018.8460953.

[58] M. Tran, L. Gabert, S. Hood, and T. Lenzi, "A lightweight robotic leg prosthesis replicating the biomechanics of the knee, ankle, and toe joint," *Sci. Robot.*, vol. 7, no. 72, Nov. 2022, Art. no. eabo3996, doi: 10.1126/scirobotics.abo3996.

[59] S. Au and H. Herr, "Powered ankle-foot prosthesis," *IEEE Robot. Autom. Mag.*, vol. 15, no. 3, pp. 52–59, Sep. 2008, doi: 10.1109/MRA.2008.927697.

[60] N. D. Reeves, M. Spanjaard, A. A. Mohagheghi, V. Baltzopoulos, and C. N. Maganaris, "Older adults employ alternative strategies to operate within their maximum capabilities when ascending stairs," *J. Electromyogr. Kinesiol.*, vol. 19, no. 2, pp. e57–e68, Apr. 2009, doi: 10.1016/j.jelekin.2007.09.009.

[61] L. L. Flynn, J. Geeroms, T. van der Hoeven, B. Vanderborght, and D. Lefeber, "VUB-CYBERLEGs CYBATHLON 2016 beta-prosthesis: Case study in control of an active two degree of freedom transfemoral prosthesis," *J. NeuroEng. Rehabil.*, vol. 15, no. 1, Dec. 2018, Art. no. 3, doi: 10.1186/s12984-017-0342-y.

[62] J. Mendez, S. Hood, A. Gunnel, and T. Lenzi, "Powered knee and ankle prosthesis with indirect volitional swing control enables level-ground walking and crossing over obstacles," *Sci. Robot.*, vol. 5, no. 44, Jul. 2020, Art. no. eaba6635, doi: 10.1126/scirobotics.aba6635.

[63] H. Eken et al., "A locomotion mode recognition algorithm using adaptive dynamic movement primitives," *IEEE Trans. Neural Syst. Rehabil. Eng.*, vol. 31, pp. 4318–4328, Oct. 2023, doi: 10.1109/TNSRE.2023.3327751.


**Ilaria Fagioli** received the B.Sc. degree in electronic engineering from the University of Perugia, Perugia, Italy, in 2019, and the M.Sc. degree in bionics engineering in 2021 from the University of Pisa, Pisa, Italy, and Scuola Superiore Sant'Anna, Pisa, where she is currently working toward the Ph.D. degree in biorobotics with Wearable Robotics Laboratory.

Her research focuses on the design, control, and verification of robotic lower limb prostheses.

**Francesco Lanotte** (Member, IEEE) received the M.Sc. degree (*cum laude*) in bionics engineering from the University of Pisa, Pisa, Italy, and Scuola Superiore Sant'Anna (SSSA), Pisa, Italy, in 2017, and the Ph.D. degree (*cum laude*) in biorobotics from SSSA, in 2021.

He is currently a Data Scientist with Technology and Innovation Hub, Shirley Ryan AbilityLab, Chicago, IL, USA. His research focuses on the validation of wearable technologies and the development of intelligent algorithms for diagnosis and prognosis in rehabilitation medicine.

**Tommaso Fiumalbi** received the B.Sc. and M.Sc. degrees in mechanical engineering from the University of Pisa, Pisa, Italy, in 2013 and 2016, respectively, and the Ph.D. degree in biorobotics from Scuola Superiore Sant'Anna (SSSA), Pisa, in 2022.

He was a Postdoctoral Researcher with Wearable Robotics Laboratory, SSSA, where he contributed to the design and development of robots for human rehab, focusing on innovative actuators and sensors for both robotic prosthesis and hand exoskeletons. He is currently working as a Process Engineer in an international pharmaceutical company.

**Andrea Baldoni** received the B.Sc. and M.Sc. degrees in mechanical engineering from the University of Perugia, Perugia, Italy, in 2011 and 2013, respectively, and the Ph.D. degree (*cum laude*) in biorobotics from Scuola Superiore Sant'Anna (SSSA), Pisa, Italy, in 2019.

He is currently a Postdoctoral Researcher with SSSA, where he leads the mechanical team of Wearable Robotics Laboratory. His main research interests include the design and development of innovative and smart mechanical solutions for highly ergonomic human–robot physical interaction in the field of wearable robotics.

**Alessandro Mazzarini** received the B.Sc. degree in biomedical engineering from Università Politecnica delle Marche, Ancona, Italy, in 2018, and the M.Sc. degree in bionics engineering in 2020 from the University of Pisa, Pisa, Italy, and Scuola Superiore Sant'Anna, Pisa, Italy, where he is currently working toward the Ph.D. degree in biorobotics with Wearable Robotics Laboratory.

His research interests include wearable robotics, prosthetics, control, and rehabilitation engineering.

**Filippo Dell'Agnello** received the B.Sc. and M.Sc. degrees in electronic engineering from the University of Pisa, Pisa, Italy, in 2012 and 2015, respectively.

In 2015 and 2016, he was an Affiliate Engineer of sensor integration with the Massachusetts Institute of Technology (CSAIL), Cambridge, MA, USA. He has been a Research Fellow with Wearable Robotics Laboratory, Scuola Superiore Sant'Anna, Pisa, since 2017, and an Electronic Research and Development Senior Advisor with IUVO Srl, Pontedera, Italy, since 2023. His research interests include the field of biomechatronics, with a focus on the design of electronic embedded solutions to sense, control, and power robotic platforms and wearable devices.

**Huseyin Eken** (Graduate Student Member, IEEE) received the B.Sc. degree in mechatronics engineering from Yildiz Technical University, Istanbul, Türkiye, in 2018, and the M.Sc. degree in bionics engineering in 2020 from the University of Pisa, Pisa, Italy, and Scuola Superiore Sant'Anna (SSSA), Pisa, where he is currently working toward the Ph.D. degree in biorobotics with Wearable Robotics Laboratory.

He is currently a Research Fellow with Wearable Robotics Laboratory, SSSA. His research interests include the design, control, and validation of lower limb prostheses and exoskeletons.

**Vito Papapicco** received the M.Sc. degree in computer science engineering from Politecnico di Bari, Bari, Italy, in 2017, and the Ph.D. degree in biorobotics from Scuola Superiore Sant'Anna, Pisa, Italy, in 2021.

He is currently with Soundsafe Care s.r.l., Milan, Italy. Throughout his career, he had experience as a Project Manager and Software Architect for the Research and Development of intelligent robotic applications in the industrial and healthcare fields.

**Tommaso Ciapetti** received the B.Sc. degree in physical therapy from the University of Florence, Florence, Italy, in 2015, and the M.Sc. degree in rehabilitation and technology from the University of Milan, Milan, Italy, in 2024.

He is currently working with rehabilitation hospital Fondazione Don Carlo Gnocchi, Firenze, Italy. His research interests include neurological rehabilitation, technologies and rehabilitation for amputees, and clinical validation of robotic devices.

**Alessandro Maselli** received the B.Sc. degree in physiotherapy and the M.Sc. degree in rehabilitation sciences of the health professions from the University of Florence, Florence, Italy, in 2014 and 2021, respectively.

He is currently a Physiotherapist working in the orthopedic and neurological areas with Campostaggia Hospital, Poggibonsi, Italy.

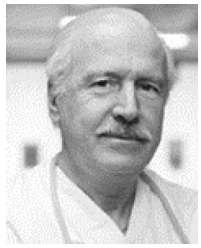

**Claudio Macchi** received the M.Sc. degree in medicine and surgery from the University of Florence, Florence, Italy, in 1979.

He has been the Director of Rehabilitation Department, Fondazione Don Gnocchi, Florence, Italy, since 2011. He has also been the Director of the U.O.F. Complex of Cardiological Rehabilitation, Fondazione Don Gnocchi, since 2002, and U.O.F. Rehabilitation Serious Brain Injury, Fondazione Don Gnocchi, since 2012. He has been a Full Professor of Physical and Rehabilitation Medicine with the University of Florence, since 2019.

**Sofia Dalmiani** received the B.Sc. degree in orthopedic techniques from the University of Bologna, Bologna, Italy, in 2021.

She is currently a certified prosthetist and orthotist with BioRobotics Institute, Scuola Superiore Sant'Anna, Pisa, Italy, and REPAIR Lab, Centro Protesi Inail, Vigorso di Budrio, Bologna, Italy. Throughout her career, she took part in the development of different smart sockets embedding EMG and vibrotactile sensors, capable of adapting their shape based on the volume of the stump of lower/limb amputees.

**Angelo Davalli** received the M.Sc. degree in electronic engineering from the University of Bologna, Bologna, Italy, in 1988, and the M.Sc. degree in medical technical sciences from Università Politecnica delle Marche, Ancona, Italy, in 2023.

He received the license as an Orthopedic Technician in 1998. He has been with Centro Protesi Inail, Vigorso di Budrio, Bologna, Italy, since 1992, initially as a Designer of upper-limb prostheses, and then as a Project Manager in several research projects focusing on innovative in upper-limb prostheses and aids for the elderly and disabled. He is currently the Head of Training and Didactics Research Area with Centro Protesi Inail, and an Adjunct Professor with the University of Bologna, Italy. He has authored more than 90 scientific publications.

**Emanuele Gruppioni** (Member, IEEE) received the M.Sc. degree in electronic engineering with biomedical specialization from the University of Bologna, Bologna, Italy, in 2006, and the degree of C.P.O. (Certified Prosthetist and Orthotist) in 2014 and the Ph.D. degree in bioengineering and bioscience from University Campus BioMedico, Rome, Italy, in 2020.

He has been a Researcher with Centro Protesi Inail, Vigorso di Budrio, Bologna, Italy, since 2006, and a Professor with the Department of Biomedical and Neuromotor Sciences, University of Bologna, since 2015. He is currently the Technical Director of Research Area with Centro Protesi Inail. His activities mainly concern prosthetic limbs and new medical devices for rehabilitation, from their design and development to the clinical studies for validation.

**Emilio Trigili** (Member, IEEE) received the M.Sc. degree in biomedical engineering from the University of Pisa, Pisa, Italy, in 2015, and the Ph.D. degree in biorobotics from Scuola Superiore Sant'Anna (SSSA), Pisa, in 2019.

He is currently an Assistant Professor of bioengineering with BioRobotics Institute, SSSA, where he is focusing on the design, control, and validation of upper- and lower limb robotic exoskeletons for rehabilitation and daily-life assistance, as well as robotic lower limb prostheses.

**Simona Crea** (Member, IEEE) received the B.Sc. and M.Sc. degrees (*cum laude*) in biomedical engineering from the University of Pisa, Pisa, Italy, in 2009 and 2012, respectively, and the Ph.D. degree (*cum laude*) in biorobotics from Scuola Superiore Sant'Anna (SSSA), Pisa, in 2015.

She is currently a tenure-track Assistant Professor of biomedical engineering with SSSA. Her research interests include wearable robotics for rehabilitation, assistance, and augmentation of human motor functions. She has authored more than 50 papers in scientific journals and serves as an Associate Editor for different scientific journals and international conferences.

**Nicola Vitiello** (Member, IEEE) received the M.Sc. degree in biomedical engineering from the University of Pisa, Pisa, Italy, in 2006, and the Ph.D. degree in biorobotics from Scuola Superiore SantAnna (SSSA), Pisa, Italy, in 2010. He is a Full Professor with The BioRobotics Institute, Scuola Superiore Sant'Anna (SSSA), Pisa, Italy, where he coleads Wearable Robotics Laboratory. He is the coauthor of more than 110 ISI/Scopus papers and coinventor of more than 25 patents/patent applications. He served as the Scientific Secretary of the EU FP7 CA-RoboCom Project, and he was the Scientific Coordinator of EU FP7 CYBERLEGs Project and the H2020-ICT-CYBERLEGs Plus projects. He is currently the scientific project coordinator of the national projects MOTU++ and BioARM, both promoted by Inail, and is a partner of the H2020-ICT-REHYB and H2020-ICT-CONBOTS projects. He is the cofounder, director, and advisor of IUVO Srl, a spin-off company of SSSA.

Open Access funding provided by 'Scuola Superiore "S.Anna" di Studi Universitari e di Perfezionamento' within the CRUI CARE Agreement